

UC Berkeley

UC Berkeley Previously Published Works

Title

Mathematical Modelling of Arctic Polygonal Tundra with Ecosys: 1. Microtopography Determines How Active Layer Depths Respond to Changes in Temperature and Precipitation

Permalink

<https://escholarship.org/uc/item/09x4k422>

Journal

Journal of Geophysical Research Biogeosciences, 122(12)

ISSN

2169-8953

Authors

Grant, RF
Mekonnen, ZA
Riley, WJ
[et al.](#)

Publication Date

2017-12-01

DOI

10.1002/2017jg004035

Peer reviewed

RESEARCH ARTICLE

10.1002/2017JG004035

This article is a companion to Grant et al. (2017), <https://doi.org/10.1002/2017JG004037>.

Key Points:

- Increases in SWC with lower surface elevation caused increases in soil thermal conductivity that caused increases in ALD of up to 15 cm
- For higher polygon features, interannual variation in ALD was more closely associated with annual precipitation than mean annual temperature
- Soil wetting from increases in precipitation may hasten permafrost degradation beyond that caused by increases in temperature

Supporting Information:

- Supporting Information S1

Correspondence to:

R. F. Grant,
rgrant@ualberta.ca

Citation:

Grant, R. F., Mekonnen, Z. A., Riley, W. J., Wainwright, H. M., Graham, D. & Torn, M. S. (2017). Mathematical modelling of arctic polygonal tundra with *ecosys*: 1. Microtopography determines how active layer depths respond to changes in temperature and precipitation. *Journal of Geophysical Research: Biogeosciences*, 122, 3161–3173. <https://doi.org/10.1002/2017JG004035>

Received 5 JUL 2017

Accepted 8 NOV 2017

Accepted article online 17 NOV 2017

Published online 20 DEC 2017

©2017. American Geophysical Union.
All Rights Reserved.

Mathematical Modelling of Arctic Polygonal Tundra with *Ecosys*: 1. Microtopography Determines How Active Layer Depths Respond to Changes in Temperature and Precipitation

R. F. Grant¹, Z. A. Mekonnen², W. J. Riley², H. M. Wainwright², D. Graham³, and M. S. Torn²

¹Department of Renewable Resources, University of Alberta, Edmonton, AB, Canada, ²Earth Science Division, Lawrence Berkeley National Laboratory, Berkeley, CA, USA, ³Environmental Sciences Division, Oak Ridge National Laboratory, Oak Ridge, TN, USA

Abstract Microtopographic variation that develops among features (troughs, rims, and centers) within polygonal landforms of coastal arctic tundra strongly affects movement of surface water and snow and thereby affects soil water contents (θ) and active layer depth (ALD). Spatial variation in ALD among these features may exceed interannual variation in ALD caused by changes in climate and so needs to be represented in projections of changes in arctic ALD. In this study, increases in near-surface θ with decreasing surface elevation among polygon features at the Barrow Experimental Observatory (BEO) were modeled from topographic effects on redistribution of surface water and snow and from lateral water exchange with a subsurface water table during a model run from 1981 to 2015. These increases in θ caused increases in thermal conductivity that in turn caused increases in soil heat fluxes and hence in ALD of up to 15 cm with lower versus higher surface elevation which were consistent with increases measured at BEO. The modeled effects of θ caused interannual variation in maximum ALD that compared well with measurements from 1985 to 2015 at the Barrow Circumpolar Active Layer Monitoring (CALM) site ($R^2 = 0.61$, RMSE = 0.03 m). For higher polygon features, interannual variation in ALD was more closely associated with annual precipitation than mean annual temperature, indicating that soil wetting from increases in precipitation may hasten permafrost degradation beyond that caused by soil warming from increases in air temperature. This degradation may be more rapid if increases in precipitation cause sustained wetting in higher features.

1. Introduction

A large part of the Arctic Coastal Plain in northern Alaska is characterized by polygonal landforms caused by seasonal freezing and thawing of tundra soil (Hinkel et al., 2005). Microtopography that develops within these landforms strongly affects surface water and snow movement and hence soil hydrologic and thermal conditions in landform features with different surface elevations, usually summarized as troughs, centers (high or low), and rims. Greater active layer depths (ALDs) and higher temperatures have been found in wetter soils under low-lying troughs than in drier soils under adjacent higher rims and centers (Gamon et al., 2012; Hubbard et al., 2013; Zona et al., 2011), likely due to greater thermal conductivity in wetter soils (Hinzman et al., 1991).

The different hydrologic and thermal conditions in the soil profiles of these features strongly affect biogeochemical processes, plant types, and productivities and hence carbon storage in polygonal landforms (Wainwright et al., 2015; Zona et al., 2011). More rapid CO₂ emissions have been recorded from rims than from troughs and centers, likely because lower water tables improved aeration in more elevated landform features (Zona et al., 2011). More rapid CH₄ emissions have been recorded from troughs and centers than from rims, indicating poorer aeration in lower landform features (Vaughn et al., 2015).

Small-scale microtopographic effects on water distribution within a landform may affect biogeochemical processes more than do large-scale differences in climates and soils across widely different landforms (Sommerkorn, 2008). Consequently, these effects must be accurately represented in process models used to study the impacts of climate change on arctic ecosystems, but apart from Kumar et al. (2016), they have usually been overlooked in modeling studies. Although there has recently been progress in three-dimensional modeling of fully coupled surface and subsurface thermal hydrology (e.g., Painter et al., 2016),

results from such modeling have not yet been tested against field measurements of soil water and ice contents in topographically variable landscapes. Here we applied a model with detailed representation of the physical processes by which heat, water, solutes, and gases are transferred vertically and laterally among features in polygonal landforms as affected by their surface elevations and soil properties. These transfers were coupled with a comprehensive simulation of the biological oxidation-reduction reactions and the C and nutrient transformations that these reactions drive. This coupling occurred through the aqueous concentrations of the reactants and products that determine the kinetics of these reactions, which were in turn determined by these transfers.

We implement and test this coupling in the ecosystem model *ecosys*, in which a comprehensive set of fully coupled biological and hydrological processes has been extensively tested against eddy covariance (EC) fluxes and related ecophysiological measurements under contrasting site and weather conditions in boreal, temperate, and tropical forests (Grant, Barr, et al., 2007; Grant, Black, et al., 2007; Grant, Barr, et al., 2009; Grant, Hutyra, et al., 2009; Grant, Margolis, et al., 2009; Grant et al., 2010), wetlands (Dimitrov et al., 2011, 2014; Grant, Desai, et al., 2012; Grant & Roulet, 2002; Mezbahuddin et al., 2014), grasslands (Grant, Baldocchi, et al., 2012; Grant & Flanagan, 2007), tundra (Grant et al., 2003, 2015, Grant, Humphreys, et al., 2011), and croplands (Grant, Arkebauer, et al., 2007; Grant, Kimball, et al., 2011). In this paper we test and apply the model in low- and flat-centered polygonal landforms at the Next Generation Ecosystem Experiment (NGEE-Arctic; <http://ngee-arctic.ornl.gov/>) site in Barrow, AK, where observations of soil hydrological and thermal conditions, surface gas and energy exchanges, and plant productivity are available.

We evaluate the hypothesis that topographic effects on movements of water and snow affect soil wetness and thereby ALD, primarily through effects on thermal conductivity. In the accompanying paper (Grant et al., 2017), we use *ecosys* to analyze whether these topographic effects on soil wetness and ALD explain variation in CO₂ exchanges, CH₄ emissions, and vegetation productivity across landscape features. This testing was intended to contribute toward a key objective of NGEE Arctic: to advance a robust predictive understanding of Earth's climate and environmental systems by delivering a process-rich ecosystem model, extending from bedrock to the top of the vegetative canopy/atmospheric interface, in which the evolution of arctic ecosystems in a changing climate can be modeled.

2. Field Experiment

2.1. Site Description

The Barrow Experimental Observatory (BEO) is located ~6 km east of Barrow, AK (71.3°N, 156.5°W) at the northern tip of Alaska's Arctic Coastal Plain. Barrow has a maritime climate characterized by long, dry winters and short, moist, cool summers, with a mean annual air temperature of –12°C and mean annual precipitation of 106 mm. Continuous ice-rich permafrost extends to >400 m depth, overlain by a shallow active layer whose depth varies spatially and interannually from approximately 20 to 60 cm. The BEO is more fully described in Dafflon et al. (2016, 2017), Vaughn et al. (2015), and Wainwright et al. (2015).

3. Model Experiment

3.1. Model Description

Key model equations and their parameterizations used to test the hypotheses in this study are described in Appendices A to H in the supporting information to this article (Table 1). These equations are cited with regard to key model processes in section 4 below. Reference to these equations in the supporting information is intended to provide insight into model behavior but is not required to understand model results. Of particular relevance to this study are equations in Appendix D: *Soil Water, Heat, Gas and Solute Fluxes* that represent physical processes governing the exchange of heat, water, and gases between ecosystem surfaces (snowpacks, litter, and soil) and the atmosphere, fully coupled with the transport of heat, water, snow, gases, and solutes in vertical and lateral directions through snowpacks, surface litter, and soil in topographically variable landscapes. These coupled processes drive transformations of heat and water through freezing and thawing in snowpacks, surface litter, and soil. Algorithms in Appendix B: *Soil-Plant Water Relations* represent physical processes driving soil-plant-atmosphere water transfer using coupled algorithms for hydraulically driven root water uptake with energy-driven canopy transpiration. All parameters in these algorithms are unchanged from those in earlier studies of forests, crops, and grasslands cited above.

Table 1
List of Appendices in the Supporting Information

Appendix	Title	Equations
A	Microbial C, N, and P Transformations	(A1)–(A39)
B	Soil-Plant Water Relations	(B1)–(B14)
C	Gross Primary Productivity, Autotrophic Respiration, Growth, and Litterfall	(C1)–(C53)
D	Soil Water, Heat, Gas, and Solute Fluxes	(D1)–(D21)
E	Solute Transformations	(E1)–(E57)
F	Symbiotic N ₂ Fixation	(F1)–(F26)
G	CH ₄ Production and Consumption	(G1)–(G27)
H	Inorganic N Transformations	(H1)–(H21)

3.2. Model Runs

We defined the *ecosys* computational domains from the polygon classification scheme of Wainwright et al. (2015), in which polygons of 5–20 m at BEO were resolved into different types based on surface elevations. The low-centered polygonal (LCP) landform was represented as a center 6 m in width and length, surrounded

by a rim 1 m in width and 0.2 m in height above the center, which was surrounded in turn by a trough 1 m in width and 0.2 m in depth below the rim (Figure 1a). The trough and the center were connected through a 1 m breach in the rim, based on the observation of Dafflon et al. (2017) that LCP ridges are variable in height. The flat-centered polygonal (FCP) landform was represented by features with the same dimensions, but the center was level with the rim (Figure 1b). The landform surfaces were thus 36% centers, 28% rims, and 36% troughs, similar to those derived from a high-resolution digital elevation model by Kumar et al. (2016). Other landforms such as high-centered polygons (HCPs) were not represented at this stage of model testing, based on the findings of Wainwright et al. (2015) that 47% of the BEO landscape is occupied by FCPs and most of the remainder by LCPs.

Soil profiles representing the key properties of the centers, rims, and troughs used in *ecosys* are given in Table 2. Measurements of these properties indicated greater variation within than among features with no consistent topographic effects on soil horization (Kumar et al., 2016). Therefore, soil properties in each feature were assumed to be the same at any depth relative to the its surface so that differences in modeled hydrological and thermal conditions among features could be attributed solely to microtopographic effects.

Each grid cell in the LCP and FCP was initialized with the same populations of sedge (200 m⁻²) and moss (10⁴ m⁻²) (Grant et al., 2015) in the model year 1980. Both model polygons were run from 1980 to 2015 using gap-filled ½-hourly meteorological data (short-wave and longwave radiation, air temperature, relative humidity, wind speed, and precipitation) from 1 January 1981 to 15 June 2013 derived by Xu and Yuan (2016) from the Barrow, AK, station of NOAA/Earth System Laboratory, Global Monitoring Division (<http://www.esrl.noaa.gov/gmd/obop/brw/>), and NOAA's National Climate Data Center, and then using 1-hourly meteorological data recorded from 16 June 2013 to 31 December 2015 at BEO by Hinzman et al. (2016b).

To check that equilibrium conditions were achieved during the model runs, another run was conducted for the LCP and FCP under repeating 1987 weather with mean annual temperature (MAT) and total

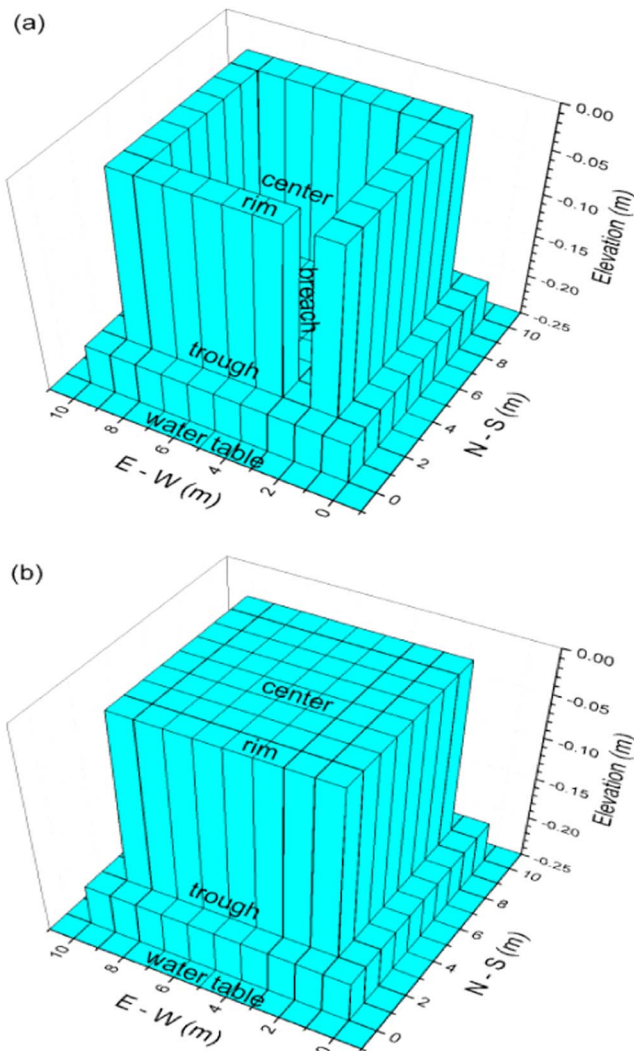


Figure 1. Representation in *ecosys* of microtopography in (a) low-centered and (b) flat-centered polygons. Elevations are expressed with respect to the rim surface.

Table 2
Key Soil Properties of the Center, Rim, and Trough Features Used in ecosystems

Depth m to bottom ^c	BD ^a Mg m ⁻³	FC ^b m ³ m ⁻³	WP ^b m ³ m ⁻³	Ksat ^b mm h ⁻¹	Sand ^a g kg ⁻¹ mineral soil	Silt ^a g kg ⁻¹ mineral soil	pH ^a	CEC Cmol kg ⁻¹	SOC ^a kg ⁻¹ soil	SON ^a g kg ⁻¹ soil	BD ^a Mg m ⁻³	FC ^b m ³ m ⁻³	WP ^b m ³ m ⁻³	Ksat ^b mm h ⁻¹	Sand ^a g kg ⁻¹ mineral soil	Silt ^a g kg ⁻¹ mineral soil	pH ^a	CEC Cmol kg ⁻¹	SOC ^a g kg ⁻¹ soil	SON ^a
0.01	0.36	0.38	0.16	16	410	318	5.55	28.1	448	17.9										
0.055	0.36	0.38	0.16	16	410	318	5.55	28.1	448	17.9										
0.1	0.42	0.38	0.16	16	410	318	5.55	28.1	395	15.8										
0.11	0.36	0.38	0.16	4.5	410	318	5.55	28.1	342	15.2										
0.155	0.36	0.38	0.16	4.5	410	318	5.55	28.1	343	15.2										
0.2	0.58	0.43	0.13	4.5	311	517	5.16	28.1	203	10.1										
0.21	0.69	0.47	0.14	22.6	311	517	5.16	28.1	135	7.7	0.36	0.38	0.16	16	410	318	5.55	28.1	448	17.9
0.255	0.77	0.47	0.14	22.6	335	382	5.16	29.9	124	8.3	0.36	0.38	0.16	16	410	318	5.55	28.1	448	17.9
0.3	0.79	0.47	0.14	22.6	335	382	5.16	20.1	121	8.1	0.42	0.43	0.13	16	410	318	5.25	28.1	395	15.8
0.31	0.64	0.43	0.14	22.6	462	68	5.16	19.7	129	8.6	0.46	0.43	0.13	4.5	410	318	5.25	28.1	342	15.2
0.355	0.55	0.39	0.08	22.6	462	68	5.16	19.7	123	8.2	0.46	0.43	0.13	4.5	410	318	5.25	28.1	343	15.2
0.4	0.36	0.25	0.11	545	361	517	5.06	19.7	166	11.1	0.58	0.43	0.13	4.5	311	517	5.16	28.1	203	10.1
0.45	0.36	0.25	0.11	545	361	517	5.06	19.7	166	11.1	0.69	0.47	0.14	22.6	311	517	5.16	28.1	135	7.7
0.5	0.36	0.25	0.11	545	361	517	5.06	19.7	166	11.1	0.77	0.47	0.14	22.6	335	382	5.16	29.9	124	8.3
0.55	0.79	0.47	0.14	22.6	335	382	5.16	20.1	121	8.1	0.79	0.47	0.14	22.6	335	382	5.16	20.1	121	8.1
0.6	0.64	0.43	0.14	545	462	68	5.16	19.7	129	8.6	0.64	0.43	0.14	545	462	68	5.16	19.7	129	8.6
0.7	0.55	0.39	0.08	545	462	68	5.16	19.7	123	8.2	0.55	0.39	0.08	545	462	68	5.16	19.7	123	8.2
0.9	0.36	0.25	0.11	545	361	517	5.06	19.7	166	11.1	0.36	0.25	0.11	545	361	517	5.06	19.7	166	11.1
1.1	0.36	0.25	0.11	545	361	517	5.06	19.7	166	11.1	0.36	0.25	0.11	545	361	517	5.06	19.7	166	11.1
1.3	0.36	0.25	0.11	545	361	517	5.06	19.7	166	11.1	0.36	0.25	0.11	545	361	517	5.06	19.7	166	11.1

Note. Layer depths are expressed relative to the rim surface.

^aMeasured from BEO soil cores. ^bDerived from water retention curves measured in HCP center by Moon and Graham (2016). ^cRelative to rim surface.

precipitation (-12.6°C and 128 mm) that closely approximated long-term averages at Barrow. Equilibrium was indicated by nearly unchanging model output (e.g., fluxes change by $<1\%/yr$) during successive years under annually repeating weather, allowing variation in model output from the production model runs to be attributed to variation in the 1981–2015 weather sequence. This equilibrium was achieved by 5 years after initialization.

During model runs, overland movements of snow and surface water within the polygonal landforms were calculated from elevation differences of snowpacks and surface water between adjacent grid cells. Snow movement was modeled such that snowpack surfaces approached a common elevation over time, and water movement was modeled from kinematic wave theory with Manning's equation for surface water flow ((D1a) and (D1b)). The LCP microtopography (Figure 1a) allowed overland snow and water movement from rims to centers and troughs and between centers and troughs through the breach. The FCP microtopography (Figure 1b) allowed overland movement from rims to troughs and hence from centers to rims. Subsurface lateral water movement within the polygonal landforms was driven by soil water potential (ψ_s) differences arising in part from elevation differences between adjacent grid cells using Green-Ampt or Richards equations for saturated or unsaturated flow (D7).

Concurrently with overland flow, surface energy exchange was calculated from first-order closure of surface energy balances for net radiation (R_n), latent heat (LE), sensible heat (H), and soil heat (G) (D11). R_n was calculated from boundary inputs for shortwave and longwave radiation using set values for albedo and emissivity of the different surfaces of the polygonal ecosystem at BEO; LE and H were modeled from surface-atmosphere vapor density and temperature gradients ((B1b)–(B1d) and (D6a) and (D6b)) driven by boundary inputs for shortwave radiation, air temperature, wind speed, and humidity and from canopy stomatal ((B2a) and (B2b)) and ground surface ((D6a) and (D6b)) resistances driven by canopy water potential (ψ_c) and ψ_s maintained from precipitation versus evapotranspiration and lateral flow.

Overland flows drove convective heat transfers between adjacent grid cells from surface temperatures and from flow volumes and heat capacities ((D12a)–(D12c)). Surface energy exchange drove conductive heat transfers between adjacent grid cells from temperature gradients ((D12a)–(D12c)) and from snow and soil thermal conductivities (de Vries, 1963) (D12d). These combined transfers drove latent heats of freezing and thawing using the general heat flux equation (D13) and hence drove active layer development within each grid cell.

Surface boundary conditions were set to allow overland flow of excess surface water from troughs at the northern and southern boundaries of the modeled polygons. Snow movement across surface boundaries was not modeled. Subsurface boundary conditions were set to allow lateral discharge and recharge of water driven by elevation differences between water tables in the troughs and an external water table set to a depth of 0.05 m below and a distance of 2.5 m from the trough surfaces at the northern and southern boundaries of the modeled polygons (Figure 1) (Grant, Desai, et al., 2012). This placement of the external water table near the troughs was suggested by observations that troughs often serve as pathways for water movement through polygonal landscapes (Liljedahl et al., 2012; Woo & Guan, 2006). An upward geothermal flux of 57 mW m^{-2} was maintained across the lower boundary (Sclater et al., 1980).

3.3. Model Tests

Spatially averaged soil water contents (θ) modeled in troughs, rims, and centers of the LCP and FCP were tested against those measured by Wood et al. (2015) at BEO during 2013 acquired from the Ngee Arctic archives (<http://ngee-arctic.ornl.gov/>). Model results for surface energy exchange were aggregated over all features in both the LCP and FCP and tested against EC measurements of surface energy exchange at BEO during 2013 by Torn et al. (2016) acquired from the Ngee Arctic archives (<http://ngee-arctic.ornl.gov/>). These tests were conducted by evaluating intercepts (a), slopes (b), correlations (R^2), and root-mean-square for differences (RMSD) from regressions of measured on modeled fluxes, representing variation in measured values not explained by the regression. A successful test would be indicated by values of a near 0, b near 1, R^2 greater than that at $p = 0.001$, and RMSD similar to variation in measured values caused by measurement uncertainty, indicating that agreement between modeled and measured values was limited by uncertainty in measured values.

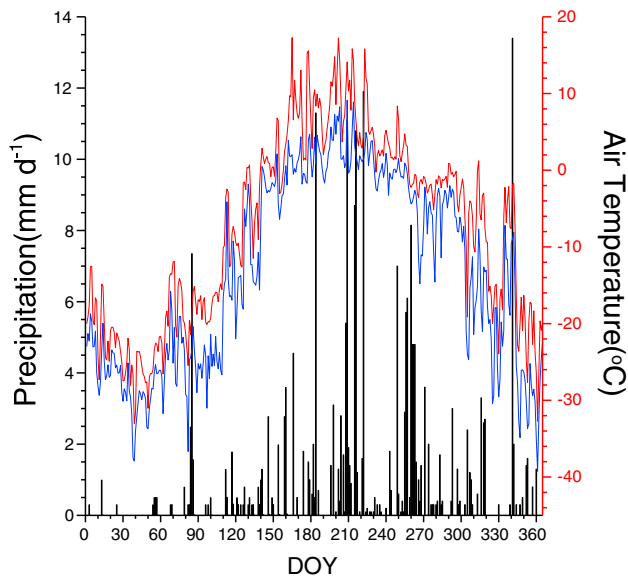


Figure 2. Daily precipitation (bars) and maximum and minimum air temperatures (lines) recorded at BEO during 2013.

Spatially averaged ALD and snow depths modeled in troughs, rims, and centers of LCPs and FCPs were visually compared with measurements of ALD by Wood et al. (2015) and of snow depth by Hinzman et al. (2016a) at BEO during 2013.

Mean air temperature (MAT) and total precipitation recorded at BEO during 2013 were -10.1°C and 213 mm, respectively, both of which were greater than long-term averages. Precipitation remained close to long-term averages until after mid-July (day of year (DOY) 200) but increased sharply thereafter (Figure 2).

4. Results and Discussion

4.1. Microtopography and Soil Water Content

Measurements of θ indicated that troughs remained near saturation during the entire growing season of 2013 in both the LCP and FCP (Figure 3). Centers remained at saturation, and rims remained near saturation in the LCP (Figure 3a), but rims dried to about two-thirds saturation and centers to one-half saturation in the FCP (Figure 3b) until more frequent precipitation caused partial rewetting after DOY 200 (Figure 2).

Most of the spatial variation of θ measured in the FCP and LCP was simulated in the model, particularly in the FCP where variation was greater (Table 3). In both landforms, root-mean-square for differences between modeled and measured values (RMSD) were similar to root-mean-square for error (RMSE) estimated from replicate measurements of θ within each feature. Soil water contents modeled in LCP troughs and centers remained at or close to saturated values, while those modeled in LCP ridges remained slightly lower than saturation during most of the growing season (Figure 3a). Values of ψ_s and hence of θ modeled in the LCP indicated that subsurface recharge approached net surface water

loss so that most of the LCP remained close to hydraulic equilibrium with the external water table set at 0.05 m below the trough surface (D10). However, ψ_s and θ modeled in the rims and centers of the FCP declined below saturated values before the onset of more frequent rainfall in late July (Figure 3b), indicating that net surface water loss exceeded subsurface recharge so that hydraulic equilibrium was not maintained between these higher features and the external water table. Consequent declines in θ allowed simulation of the soil drying measured in the higher features of the FCP.

4.2. Microtopography and Surface Energy Exchange

Surface energy fluxes (R_n , LE , H , and G) were summed from those modeled at soil, residue, sedge, and moss surfaces ((B1a) and (D11)) in each grid cell and then aggregated over all grid cells in both the LCP and FCP. These aggregated values were then averaged for comparison with EC measurements. Modeled R_n closely followed measured values (Figure 4 and Table 4). Modeled LE fluxes were similar to measured values, and modeled H fluxes were slightly higher as indicated by slopes close to 1 and less than 1, respectively (Figure 4 and Table 4). Differences between modeled and measured values were about twice the uncertainty in measured values estimated by Billesbach (2011) for both LE and H (Table 4), indicating a small model bias in partitioning R_n to H versus LE . Modeled G exceeded measured values (slope less than 1 in Table 4), particularly during sharp rises in early morning air temperatures when the soil was wet and hence thermal conductivity greater (e.g., DOY 199, 202, and 223 in Figure 4). However, the very

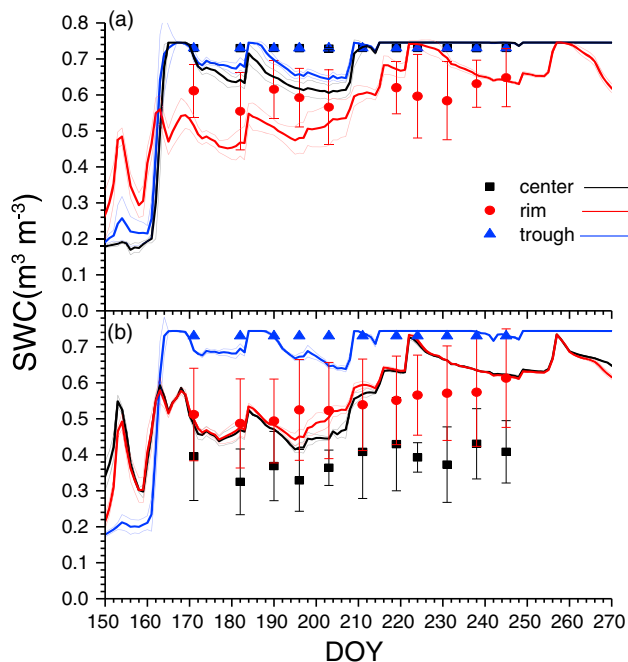


Figure 3. Soil water contents measured (symbols) and modeled (lines) at 5 cm in centers, rims, and troughs of (a) LCPs and (b) FCPs during the 2013 growing season. Lighter lines indicate standard deviations of values modeled in the grid cells of each feature (see Figure 1). Measured data from Wood et al. (2015).

Table 3
 Statistics From Regressions of Soil Water Content (θ) Measured by Wood et al. (2015) on Those Modeled by ecosys in LCP and FCP Landforms at BEO During 2013

θ Landform	a^a $m^3 m^{-3}$	b^a	R^2	RMSD ^b $m^3 m^{-3}$	RMSE ^c $m^3 m^{-3}$	n
LCP	0.37	0.47	0.44*	0.05	0.05	32
FCP	-0.05	0.99	0.72*	0.10	0.09	33

^a $Y = a + bX$ from regression of measured Y on simulated X . ^bRMSD from regression of measured Y on simulated X . ^cRMSE estimated from replication in measured values.

*Significant at $p < 0.001$.

small spatial scale of soil heat flux measurements limited the comparability of measured and modeled G .

The slight drying modeled in rims versus troughs and low centers of the LCP before the onset of more frequent rainfall in late July caused small reductions in thermal conductivity modeled in surface litter and near-surface soil of rims (D12d). These reductions caused slightly less surface energy to be partitioned to G ($10\text{--}20\text{ W m}^{-2}$) (D12c) and hence more to H (D11), in rims than in troughs and centers of the LCP (Figure 5a). The greater drying modeled in rims and centers in the FCP caused less surface energy to be partitioned to G ($20\text{--}40\text{ W m}^{-2}$) and hence more to H , in the rims and centers than in the troughs (Figure 5b). Rewetting of

centers and rims following the onset of more frequent rainfall after mid-July eliminated most of these differences in thermal conductivity and hence in energy partitioning among troughs, centers, and rims later in the year.

4.3. Microtopography and ALD

The small reductions in G modeled with slight drying of rims in the LCP (Figures 3a and 5a) had little effect on ALD of rims (Figure 6c) versus troughs and centers (Figures 6a and 6e). The greater reductions in G modeled with greater drying in the rims and centers of the FCP before DOY 210 (Figures 3b and 5b) slowed active layer development and caused shallower ALD (Figures 6d and 6f versus Figure 6b).

Topographic effects on snow redistribution within each landform caused snowpacks modeled on different features in the FCP to be deeper than those in the LCP (Figure 7b versus Figure 7a) because the greater proportion of more versus less elevated features in the FCP (Figure 1b versus Figure 1a) enabled a uniform snow surface elevation to be achieved with less snow redistribution. However, the very deep snowpacks measured in FCP troughs were not simulated from the available meteorological data, suggesting that snow redistribution may have occurred on a larger spatial scale than that in the model or that the difference in elevation between the center and trough at the site of snow measurement was greater than that in the model (0.2 m). The greater proportion of elevated features in the FCP also slowed lateral recharge, causing FCP centers to be drier during spring and summer (Figure 3b versus Figure 3a) and therefore to accumulate less shallow ice in winter (Figure 6f versus Figure 6e). Greater G efflux with greater thermal conductance in shallow snowpacks during winter (D12) and smaller G influx with smaller thermal conductance in drier soil surfaces during spring and early summer (Figure 5b) caused ALD modeled in FCP centers to be ~ 5 cm shallower than those in the troughs (Figure 7b).

Model results indicated that topographic effects of landform features (troughs, rims, and centers) on θ (section 4.1) determined those on surface energy exchange (section 4.2) and hence ALD (section 4.3) in the LCP and FCP. Topographic effects on surface snow and water redistribution influenced ALD in the model through several processes:

4.4. Modeling the Effects of Microtopography on Spatial Variation in ALD

Model results indicated that topographic effects of landform features (troughs, rims, and centers) on θ (section 4.1) determined those on surface energy exchange (section 4.2) and hence ALD (section 4.3) in the LCP and FCP. Topographic effects on surface snow and water redistribution influenced ALD in the model through several processes:

1. Topographic effects on redistribution of snow in winter and of surface water during snowmelt and periods of excess precipitation in spring and summer (Figure 7) caused wetting of lower features and drying of higher features (Figure 3), altering thermal conductivity, and hence G (Figure 5), and hence active layer development (Figure 6).
2. Infiltration of redistributed surface water advected heat into the soil profiles of lower features ((D12a)–(D2c)) further hastening active

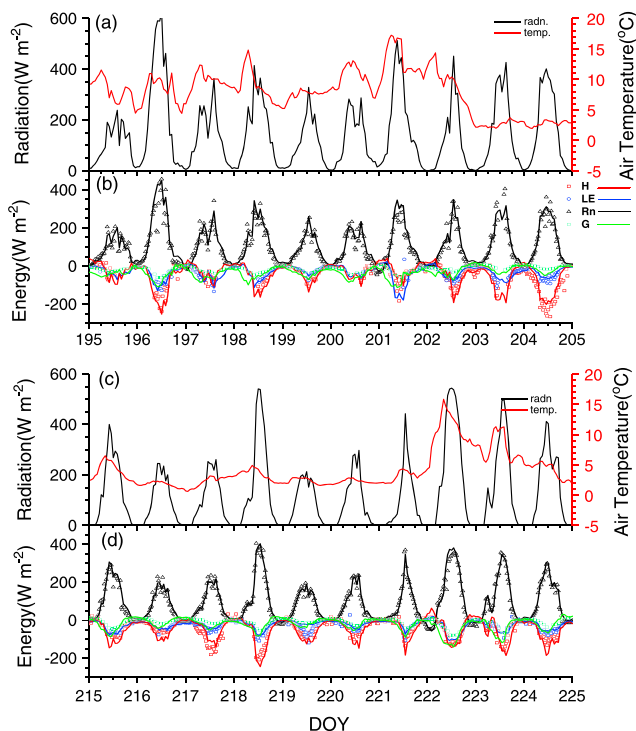


Figure 4. (a, c) Radiation and air temperatures recorded and (b, d) energy exchange measured (symbols) and modeled (lines) during late July (Figures 4a and 4b) and early August (Figures 4c and 4d) 2013 at BEO. Measured fluxes from Torn et al. (2016). For fluxes, positive values indicate influxes and negative values effluxes.

Table 4
 Statistics From Regressions of Hourly Averaged Net Radiation (R_n), Latent (LE), Sensible (H), and Soil (G) Heat Fluxes Measured by Torn et al. (2016) on Those Modeled Over Combined LCP and FCP Landforms at BEO During 2013

Flux	a^a	b^a	R^2	RMSD ^b	RMSE ^c	n
	$W\ m^{-2}$					
R_n	-8	0.98	0.97*	13	na	2,464
LE	1	0.98	0.76*	11	6	925
H	-5	0.73	0.78*	19	9	1,519
G	0	0.38	0.58*	8	na	2,464

^a $Y = a + bX$ from regression of measured Y on simulated X . ^bRMSD from regression of measured Y on simulated X . ^cRMSE estimated from EC measurements by Billesbach (2011).
 *Significant at $p < 0.001$.

- layer development, as modeled in an earlier study (Grant et al., 2015).
- Deeper snowpacks were modeled in lower versus higher features (Figure 7), consistent with the snow survey data at BEO (Wainwright et al., 2017). These deeper snowpacks reduced thermal conductance and hence G modeled from soil to snowpack during winter (D12c), which caused slower soil freezing and hence greater persistence of the active layer in lower features during winter (Figures 6a, 6b, and 6e versus Figures 6c, 6d, and 6f).
- Redistribution of snow and surface water caused large volumes of shallow ground ice to be modeled in lower features, which was consistent with ice volumes of up to 80% found at Barrow by Kanevskiy et al. (2013). Similarly, Wainwright et al. (2015) detected the presence of massive ground ice or ice-rich permafrost in LCPs at BEO.
- Deeper snowpacks and greater soil ice content modeled in lower features increased thermal requirements for melting (D13) and so delayed the onset of soil thawing in spring. Consequently, active layer development started later but progressed more rapidly in lower, wetter features (Figures 7a and 7b), as was measured at BEO by Zona et al. (2009) and Dafflon et al. (2017).

Topographic effects on subsurface lateral water transfer also influenced ALD in the model through several processes:

- Elevation of each landform feature above the external water table surrounding the troughs (Figure 1) determined the soil water potential (ψ_s) at which θ equilibrated with the external water table (D10). This equilibrium was maintained in the modeled LCP because differences between precipitation and evapotranspiration in each feature were offset by discharge and recharge through lateral flow in saturated, ice-free zones between the feature and the external water table. The formation of these zones required sufficient heat flux (D13) to melt all ice (D8). In these zones, lateral hydraulic conductivity was large (Table 2) and soil matric water potential was near its saturated value, so that differences in ψ_s were mostly determined by those in elevation. These zones started to develop in the LCP when soil in the troughs and low centers thawed below the depth of the external water table (0.05 m below the trough surfaces in Figure 1a) and when the soil in the rims thawed below the surface of adjacent troughs or low centers (0.2 m below the rim surface in Figure 1a). If thawing did not extend below these depths, soil porosity of troughs and low centers at the depth of the external water table, or of rims at the depths of the surfaces

adjacent to troughs or low centers, was fully occupied by ice and water, preventing lateral flow. Thus, direct contact between troughs and low centers through the breach in the LCP (Figure 1a) hastened recharge through lateral flow from troughs through the breach to low centers and then from low centers to rims, enabling ψ_s and hence θ of all landform features to remain close to hydraulic equilibrium with the external water table during the thaw period (Figure 3a).

- Hydraulic equilibrium with the external water table was not maintained in the FCP because saturated, ice-free zones through which lateral flow to rims and flat centers could occur either did not develop or developed more slowly than those in the LCP. The slower development of these zones was attributed in the model to greater elevation (Figure 1b) and reduced thermal conductivity of flat centers which delayed or prevented thawing below adjacent troughs.

The absence or reduced development of saturated, ice-free zones caused higher features in the FCP to become hydrologically isolated from the external water table, as observed in polygonal landscapes by Liljedahl et al. (2012). Consequently ψ_s and hence θ modeled in

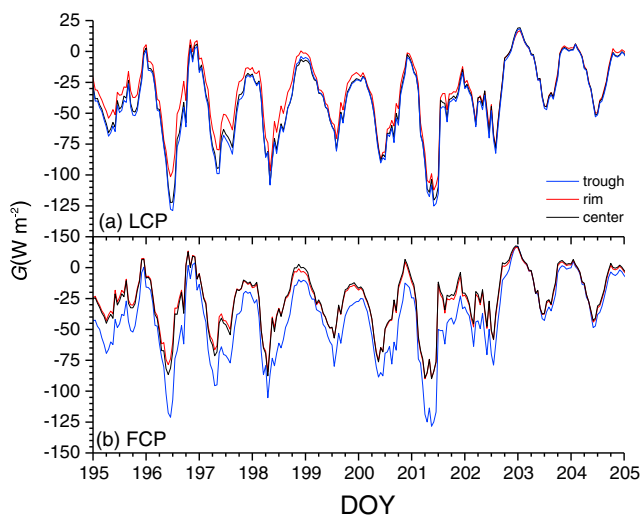


Figure 5. Soil (G) heat fluxes modeled in troughs, centers, and rims of the (a) LCP and (b) FCP during late July 2013 at BEO. Positive values indicate losses, and negative values represent gains.

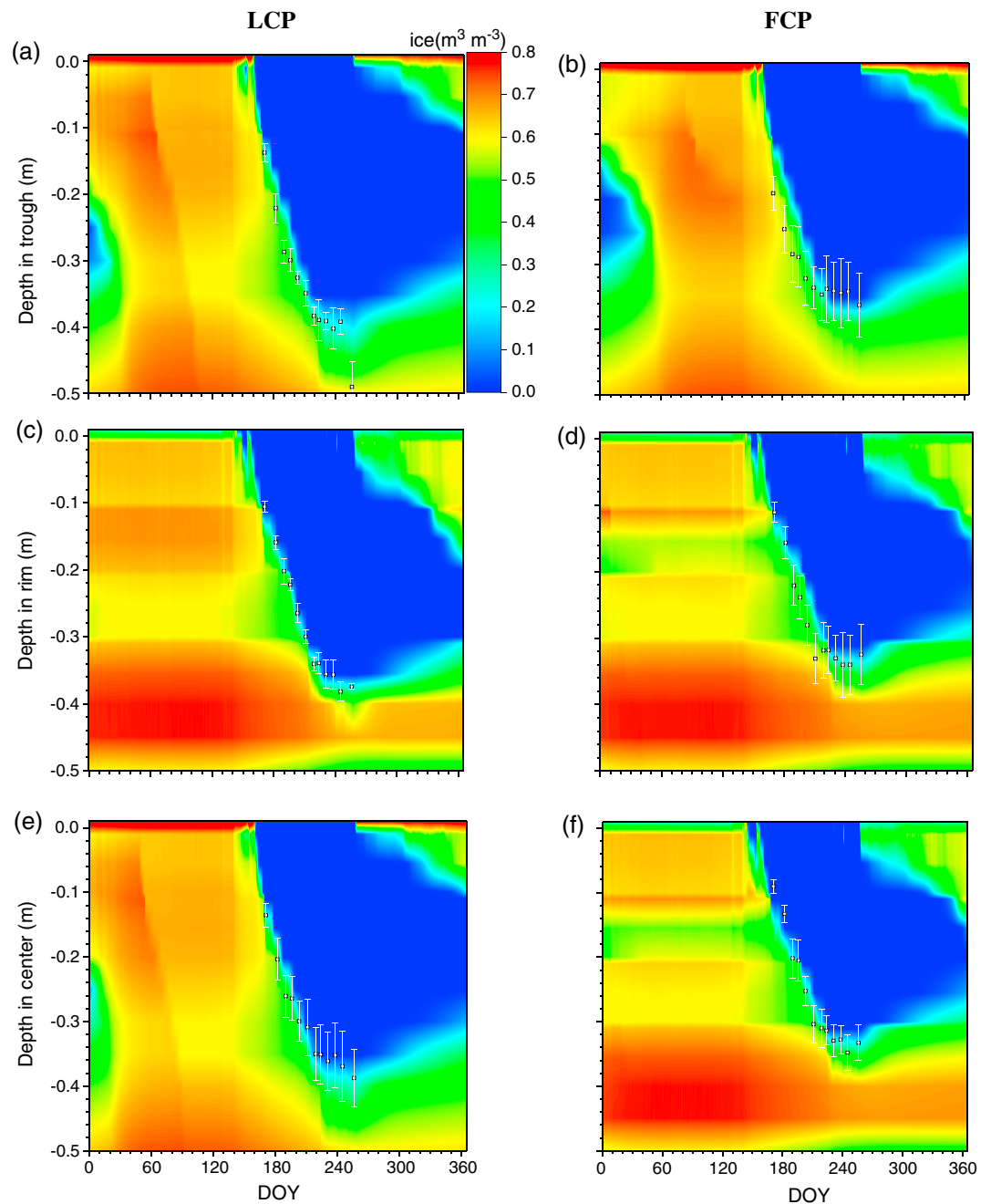


Figure 6. Ice contents of surface litter and soil profiles modeled during 2013 in trough (a, b), rim (c, d), and center (e, f) features of the LCP (Figures 6a, 6c, and 6e) and FCP (Figures 6b, 6d, and 6f). Active layers are indicated by ice-free zones in dark blue. Symbols represent measurements of ALD from Wood et al. (2015).

the rims and centers of the FCP declined below equilibrium values with the external water table (Figure 3b) because recharge through lateral flow from the external water table to these features was too slow to offset excesses of evapotranspiration over precipitation during periods with infrequent rainfall (e.g., before DOY200 in Figure 2).

4.5. Microtopography and Interannual Variation in ALD

Weather data from 1981 to 2015 for Barrow, AK, derived by Xu and Yuan (2016) and recorded by Hinzman et al. (2016b) indicated gradually rising MAT ($0.1^{\circ}\text{C yr}^{-1}$ $P < 0.001$) and precipitation (1.9 mm yr^{-1} $P = 0.002$) (Figure 8a). ALDs modeled under historically average MAT and precipitation, represented by repeating 1987

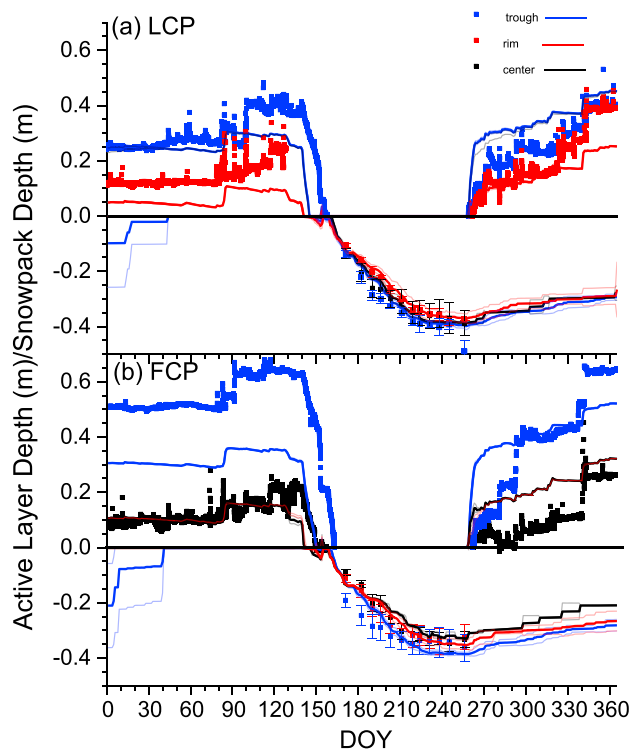


Figure 7. (a) Snowpack and active layer depths measured (symbols) and modeled (lines) in troughs, centers, and rims of the (a) LCP and (b) FCP at BEO in 2013. Faint lines indicate standard deviation of values modeled in all grid cells of each feature.

weather, remained stable in all features of the LCP and FCP from 1985 to 2015, indicating that the model had achieved thermal and hydrological equilibrium under the site conditions at Barrow within the first 5 years of the model runs. Interannual variation in ALD modeled from 1985 to 2015 (Figures 8b and 8c) could therefore be attributed to that in the weather data for Barrow (Figure 8a).

ALD modeled from 1985 to 2015 remained close to historical averages (~30 cm) until 2009, after which sustained rises in MAT and precipitation (Figure 8a) caused modeled ALD (Figures 8b and 8c) to exceed historical averages, particularly with gradual wetting of higher features (rims in the LCP and rims and centers in the FCP). ALDs modeled in lower features (LCP centers and troughs and FCP troughs) of both landforms from 1985 to 2015 varied between ~25 and 40 cm, increasing with rises in MAT (1989, 1998, and 2009–2015) and precipitation (2004 and 2009–2014) and decreasing with declines in MAT and precipitation (1991–1992 and 1995) (Figure 8b).

Interannual variation in spatially averaged ALDs modeled in LCP troughs and centers from 1991 to 2015 was correlated with that measured at the Circumpolar Active Layer Monitoring (CALM) site in BEO (<https://www2.gwu.edu/~calm/data/north.html> accessed 27 April 2017) ($R^2 = 0.61$, $P < 0.001$, RMSE = 0.03 m in Figure 8a). ALDs modeled in higher features (LCP rims and FCP rims and centers) were shallower than those in lower features by ~15 cm (Figure 8c), because they were drier (Figure 3b) and so conducted less heat into the soil (Figure 5b). ALDs modeled in these features increased with wetting from rises in precipitation (e.g., 1989, 2000, and 2010–2014) (Figures 8b and 8c).

The relationship between interannual variation in ALD and those in MAT and annual precipitation differed among landform features. ALDs modeled in LCP and FCP troughs were better correlated with MAT than with precipitation, but ALDs modeled in centers and rims were better correlated with precipitation than with MAT, particularly in the FCP (Table 5).

4.6. Modeling the Effects of Microtopography on Interannual Variation in ALD

Redistribution of snow and excess surface water, and subsurface exchange of water with the external water table, caused θ modeled in lower features to be maintained at or close to saturation from 1985 to 2015 (e.g., Figure 3) which enabled modeled ALD to remain within a range of 30 to 40 cm. These same processes caused declines in θ to be modeled in higher features (Figure 3) which reduced ALD during drier years, particularly in the FCP (Figure 8). However, ALD modeled in higher features rose sharply with rewetting from increases in precipitation (Figure 8a), because increases in G hastened thawing and consequently recharge, thereby reducing spatial variability during wetter years (Figures 8b and 8c). ALD of these higher features in the model was thus sensitive to precipitation (Table 5) and to subsurface hydrology through the processes described in section 4.4 above.

4.7. Comparing Modeled and Observed Effects of Microtopography on Spatial Variation in ALD

The processes described in section 4.4 allowed the model to simulate slightly greater ALD in troughs and centers than in rims of the LCP (Figure 8b), and in troughs than in rims and centers of the FCP (Figure 8c) during 2013, which was consistent with measurements at BEO (Figures 6 and 7). However, model results indicated that the small differences in ALD currently measured among features may have been caused by landscape wetting with increased precipitation since 2009. This modeled wetting increased ALD in higher features more than in lower, reducing differences in ALD modeled among features from those modeled earlier. Average ALD modeled in LCP rims and centers during 2008 were 21 and 28 cm, close to values of 22 and 28 cm measured in coastal polygonal tundra by Zona et al. (2011). Average ALDs modeled in 2011 increased from 28 cm in FCP rims to 39 cm in LCP troughs, consistent with increases in ALDs measured at BEO in 2011 by Gangodagamage et al. (2014) from 33 cm in FCP rims to 48 cm in LCP troughs.

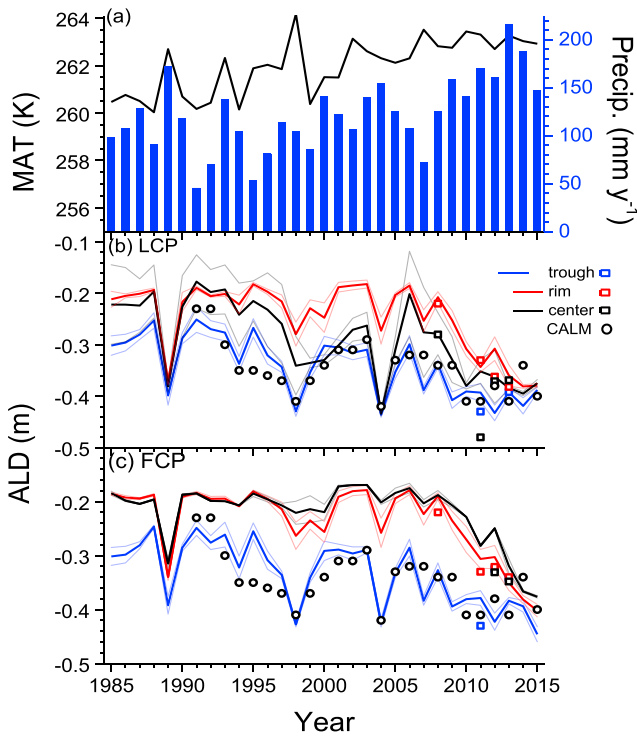


Figure 8. (a) Mean annual temperature (line) and annual precipitation (bars) at Barrow, AK, from Xu and Yuan (2016) from 1985 to 15 June 2013 and from Hinzman et al. (2016b) thereafter and active layer depth (ALD) modeled (lines) on 31 August in troughs, rims, and centers of the (b) LCP and (c) FCP and measured in late August 1991–2009 at the CALM site in BEO (open circles), late August 2008 by Zona et al. (2011), and in early September 2012–2013 by Wood et al. (2015) (open squares). Faint lines indicate standard deviation of values modeled for all grid cells in each feature.

These increases in ALD were modeled from a reduction of 20 cm in elevation above a common external water table. Increases in ALD from 22 cm in higher features to 39 cm in lower features modeled on 31 August 2007 (Figures 8b and 8c) corresponded to increases from 27 cm to 36 cm measured by Kim (2015) in mid-September 2007 with a 6 cm reduction in elevation above the water table during a flooding experiment at BEO. The range in ALD modeled among landform features during 2011 was 28–42 cm, average 36 cm (Figures 8b and 8c), consistent with a range of 21–58 cm, average 36 cm derived by Hubbard et al. (2013) from geophysical measurements along a 475 m transect in late September 2011 at BEO. Both modeled and measured ALD in 2011 were greater at lower elevations, with an average \pm SD of 38 ± 3 cm modeled in the LCP versus 43 ± 12 cm derived from geophysical measurements in LCPs, than at higher, with an average \pm SD of 34 ± 4 cm modeled in the FCP versus 32 ± 9 cm derived from geophysical measurements in HCPs. Thus, elevation was a key determinant of ALD until at least 2011.

Increases in ALD with soil wetness have not been simulated in some earlier modeling studies. Atchley et al. (2016) used a one-dimensional integrated surface/subsurface permafrost thermal hydrology model to predict that ALD was relatively insensitive to the amount of water on polygonal landscape features as determined by set changes in water table depths. In this model the effects of soil wetness on thermal conductivity for heat transfer were largely offset by those on thermal requirements for melting ice during active layer development. In our three-dimensional modeling study, however, the effects of water influxes on heat transfer through advection and thermal conductivity were greater than those on thermal requirements for melting.

4.8. Comparing Modeled and Observed Effects of Microtopography on Interannual Variation in ALD

The modeled response of interannual variation in ALD to precipitation was consistent with a finding from Olivas et al. (2011) that ALD measured in a warm, dry year (e.g., 2007) can be less than that during a cool, wet year (e.g., 2004). This model response was also consistent with observations at the two CALM sites near Barrow where MAT has been rising for several decades, but sustained increases in ALD have only occurred since 2005 (Gangodagamage et al., 2014) after which precipitation has gradually increased (Figure 8a).

Detection of long-term changes in ALD to corroborate these model results is complex. Luo et al. (2016) found only small increases in ALD (0.05 cm yr^{-1}) at the Barrow CALM sites since the early 1990s, likely due to surface subsidence caused by deeper permafrost thawing which can offset increases in ALD. Ecosys does not currently simulate surface subsidence, but work is in progress to do so.

Increases in ALD with precipitation as modeled in this study (Figure 8 and Table 5) are likely a general phenomenon. Iijima et al. (2010) observed increases in ALD of 20 cm during 3 years of higher precipitation at study sites in eastern Siberia which they attributed to increased thermal conductivity and heat capacity of wetter soil. Such increases indicate that projected rises in precipitation during the next century (Bintanja & Selten, 2014) may hasten increases in ALD of polygonal tundra beyond those from accompanying rises in MAT, as was modeled in an earlier study of an arctic landscape (Grant, 2015). These increases will likely be larger in higher features of polygonal tundra if rising precipitation causes sustained wetting of higher features.

Table 5
Correlations of Active Layer Depth (ALD) Modeled on 31 August With Mean Annual Temperature (MAT) and Annual Precipitation at Barrow, AK, From 1985 to 2015

Feature	MAT		Precipitation	
	R ²	P	R ²	P
	LCP			
Troughs	0.50	<0.001	0.38	<0.001
Centers	0.37	0.003	0.53	<0.001
Rims	0.30	0.001	0.52	<0.001
	FCP			
Troughs	0.45	<0.001	0.34	<0.001
Centers	0.16	0.027	0.42	<0.001
Rims	0.26	0.003	0.50	<0.001

5. Summary

1. Topographic effects on redistribution of surface water and snow and on lateral water exchange with a subsurface water table enabled greater θ to be modeled in lower versus higher features of polygonal landforms in an arctic tundra.
2. Greater θ caused greater G to be modeled in lower versus higher features.
3. Greater G caused greater ALD to be modeled in lower versus higher features.
4. The effects of θ on G caused greater ALD to be modeled in wetter years than in drier, particularly with wetting of higher features.
5. These model results indicate the importance of water from precipitation, surface redistribution, and subsurface transport on ALD in polygonal tundra with complex microtopography.

Acknowledgments

This research was supported by the Director, Office of Science, Office of Biological and Environmental Research of the U.S. Department of Energy under contract DE-AC02-05CH11231 to Lawrence Berkeley National Laboratory as part of the Next-Generation Ecosystem Experiments in the Arctic (NGEE-Arctic) project. Data used in this paper are available from the NGEE website as cited in the text.

References

- Atchley, A. L., Coon, E. T., Painter, S. L., Harp, D. R., & Wilson, C. J. (2016). Influences and interactions of inundation, peat, and snow on active layer thickness. *Geophysical Research Letters*, *43*(10), 5116–5123. <https://doi.org/10.1002/2016GL068550>
- Billesbach, D. P. (2011). Estimating uncertainties in individual eddy covariance flux measurements: A comparison of methods and a proposed new method. *Agricultural and Forest Meteorology*, *151*(3), 394–405. <https://doi.org/10.1016/j.agrformet.2010.12.001>
- Bintanja, R., & Selten, F. M. (2014). Future increases in Arctic precipitation linked to local evaporation and sea-ice retreat. *Nature*, *509*(7501), 479–482. <https://doi.org/10.1038/nature13259>
- Dafflon, B., Hubbard, S., Ulrich, C., Peterson, J., Wu, Y., Wainwright, H., & Kneafsey, T. J. (2016). Geophysical estimation of shallow permafrost distribution and properties in an ice-wedge polygon-dominated Arctic tundra region. *Geophysics*, *81*(1), WA247–WA263. <https://doi.org/10.1190/geo2015-0175.1>
- Dafflon, B., Oktem, R., Peterson, J., Ulrich, C., Tran, A. P., Romanovsky, V., & Hubbard, S. S. (2017). Coincident aboveground and belowground autonomous monitoring to quantify covariability in permafrost, soil, and vegetation properties in Arctic tundra. *Journal of Geophysical Research: Biogeosciences*, *122*, 1321–1342. <https://doi.org/10.1002/2016JG003724>
- de Vries, D. A. (1963). Thermal properties of soils. In R. van Wijk (Ed.), *Physics of plant environment* (pp. 210–235). Amsterdam, Netherlands: North Holland Publishing Co.
- Dimitrov, D. D., Bhatti, J. S., & Grant, R. F. (2014). The transition zones (ecotone) between boreal forests and peatlands: Ecological controls on ecosystem productivity along a transition zone between upland black spruce forest and a poor forested fen in central Saskatchewan. *Ecological Modelling*, *291*, 96–108. <https://doi.org/10.1016/j.ecolmodel.2014.07.020>
- Dimitrov, D. D., Grant, R. F., LaFleur, P. M., & Humphreys, E. (2011). Modelling the effects of hydrology on gross primary productivity and net ecosystem productivity at Mer Bleue bog. *Journal of Geophysical Research*, *116*, G04010. <https://doi.org/10.1029/2010JG001586>
- Gamon, J. A., Kershaw, G. P., Williamson, S., & Hik, D. S. (2012). Microtopographic patterns in an arctic baydjarakh field: Do fine-grain patterns enforce landscape stability? *Environmental Research Letters*, *7*(1), 015502. <https://doi.org/10.1088/1748-9326/7/1/015502>
- Gangodagamage, C., Rowland, J. C., Hubbard, S. S., Brumby, S. P., Liljedahl, A. K., Wainwright, H., ... Wullschlegler, S. D. (2014). Extrapolating active layer thickness measurements across Arctic polygonal terrain using LiDAR and NDVI data sets. *Water Resources Research*, *50*(8), 6339–6357. <https://doi.org/10.1002/2013WR014283>
- Grant, R. F. (2015). Ecosystem CO₂ and CH₄ exchange in a mixed tundra and a fen within a hydrologically diverse Arctic landscape. Part II. Modelled impacts of climate change. *Journal of Geophysical Research: Biogeosciences*, *120*, 1388–1406. <https://doi.org/10.1002/2014JG002889>
- Grant, R. F., Arkebauer, T. J., Dobermann, A., Hubbard, K. G., Schimelfenig, T. T., Suyker, A. E., ... Walters, D. T. (2007). Net biome productivity of irrigated and rainfed maize-soybean rotations: Modelling vs. measurements. *Agronomy Journal*, *99*(6), 1404–1423. <https://doi.org/10.2134/agronj2006.0308>
- Grant, R. F., Baldocchi, D. D., & Ma, S. (2012). Ecological controls on net ecosystem productivity of a Mediterranean grassland under current and future climates. *Agricultural and Forest Meteorology*, *152*, 189–200. <https://doi.org/10.1016/j.agrformet.2011.09.012>
- Grant, R. F., Barr, A. G., Black, T. A., Gaumont-Guay, D., Iwashita, H., Kidson, J., ... Shashkov, A. (2007). Net ecosystem productivity of boreal jack pine stands regenerating from clearcutting under current and future climates. *Global Change Biology*, *13*(7), 1423–1440. <https://doi.org/10.1111/j.1365-2486.2007.01363.x>
- Grant, R. F., Barr, A. G., Black, T. A., Margolis, H. A., Dunn, A. L., Metsaranta, J., ... Bourque, C. P.-A. (2009). Interannual variation in net ecosystem productivity of Canadian forests as affected by regional weather patterns—A Fluxnet-Canada synthesis. *Agricultural and Forest Meteorology*, *149*(11), 2022–2039. <https://doi.org/10.1016/j.agrformet.2009.07.010>
- Grant, R. F., Barr, A. G., Black, T. A., Margolis, H. A., McCaughey, J. H., & Trofymow, J. A. (2010). Net ecosystem productivity of temperate and boreal forests after clearcutting—A Fluxnet-Canada synthesis. *Tellus B*, *62B*, 475–496.
- Grant, R. F., Black, T. A., Humphreys, E. R., & Morgenstern, K. (2007). Changes in net ecosystem productivity with forest age following clearcutting of a coastal Douglas fir forest: Testing a mathematical model with eddy covariance measurements along a forest chronosequence. *Tree Physiology*, *27*(1), 115–131. <https://doi.org/10.1093/treephys/27.1.115>
- Grant, R. F., Desai, A., & Sulman, B. (2012). Modelling contrasting responses of wetland productivity to changes in water table depth. *Biogeosciences*, *9*(11), 4215–4231. <https://doi.org/10.5194/bg-9-4215-2012>
- Grant, R. F., & Flanagan, L. B. (2007). Modeling stomatal and nonstomatal effects of water deficits on CO₂ fixation in a semiarid grassland. *Journal of Geophysical Research*, *112*, G03011. <https://doi.org/10.1029/2006JG000302>
- Grant, R. F., Humphreys, E. R., & Lafleur, P. M. (2015). Ecosystem CO₂ and CH₄ exchange in a mixed tundra and a fen within a hydrologically diverse Arctic landscape: Part I. Modelling vs. measurements. *Journal of Geophysical Research: Biogeosciences*, *120*, 1366–1387. <https://doi.org/10.1002/2014JG002888>
- Grant, R. F., Humphreys, E. R., Lafleur, P. M., & Dimitrov, D. D. (2011). Ecological controls on net ecosystem productivity of a mesic Arctic tundra under current and future climates. *Journal of Geophysical Research*, *116*, G01031. <https://doi.org/10.1029/2010JG001555>
- Grant, R. F., Hutyrá, L. R., de Oliveira, R. C., Munger, J. W., Saleska, S. R., & Wofsy, S. C. (2009). Modeling the carbon balance of Amazonian rain forests: Resolving ecological controls on net ecosystem productivity. *Ecological Monographs*, *79*(3), 445–463.

- Grant, R. F., Kimball, B. A., Conley, M. M., White, J. W., Wall, G. W., & Ottman, M. J. (2011). Controlled warming effects on wheat growth and yield: Field measurements and modeling. *Agronomy Journal*, *103*(6), 1742–1754. <https://doi.org/10.2134/agronj2011.0158>
- Grant, R. F., Margolis, H. A., Barr, A. G., Black, T. A., Dunn, A. L., Bernier, P. Y., & Bergeron, O. (2009). Changes in net ecosystem productivity of boreal black spruce stands in response to changes in temperature at diurnal and seasonal time scales. *Tree Physiology*, *29*(1), 1–17. <https://doi.org/10.1093/treephys/tpn004>
- Grant, R. F., Mekonnen, Z. A., Riley, W. J., Arora, B., & Torn, M. S. (2017). Mathematical modelling of arctic polygonal tundra with *ecosys*: 2. Microtopography determines how CO₂ and CH₄ exchange responds to changes in temperature and precipitation. *Journal of Geophysical Research: Biogeosciences*, *122*, 3174–3187. <https://doi.org/10.1002/2017JG004037>
- Grant, R. F., Oechel, W. C., Ping, C., & Kwon, H. (2003). Carbon balance of coastal Arctic tundra under changing climate. *Global Change Biology*, *9*(1), 16–36. <https://doi.org/10.1046/j.1365-2486.2003.00549.x>
- Grant, R. F., & Roulet, N. T. (2002). Methane efflux from boreal wetlands: Theory and testing of the ecosystem model *ecosys* with chamber and tower flux measurements. *Global Biogeochemical Cycles*, *16*(4), 1054. <https://doi.org/10.1029/2001GB001702>
- Hinkel, K. M., Frohn, R. C., Nelson, F. E., Eisner, W. R., & Beck, R. A. (2005). Morphometric and spatial analysis of thaw lakes and drained thaw lake basins in the western Arctic Coastal Plain, Alaska. *Permafrost and Periglacial Processes*, *16*(4), 327–341. <https://doi.org/10.1002/ppp.532>
- Hinzman, L. D., Kane, D. L., Benson, C. S., & Everett, K. R. (1991). Hydrologic and thermal properties of the active layer in the Alaskan Arctic. *Cold Regions Science and Technology*, *19*(2), 95–110. [https://doi.org/10.1016/0165-232X\(91\)90001-W](https://doi.org/10.1016/0165-232X(91)90001-W)
- Hinzman, L., Romanovsky, V., Cable, W., & Busey, G. (2016a). Continuous snow depth, intensive site 1, Barrow, Alaska. Retrieved from <http://ngee-arctic.ornl.gov/>, accessed 21.6.2016.
- Hinzman, L., Romanovsky, V., Cable, W., & Busey, G. (2016b). Surface meteorology, Barrow, Alaska, Area S, B, C and D, ongoing from 2012. Retrieved from <http://ngee-arctic.ornl.gov/>, accessed 19 January 2016.
- Hubbard, S. S., Gangodagamage, C., Dafflon, B., Wainwright, H., Peterson, J., Gusmeroli, A., ... Wulschleger, S. D. (2013). Quantifying and relating land-surface and subsurface variability in permafrost environments using LiDAR and surface geophysical datasets. *Hydrogeology Journal*, *21*(1), 149–169. <https://doi.org/10.1007/s10040-012-0939-y>
- Iijima, Y., Ohta, T., Kotani, A., Fedorov, A. N., Kodama, Y., & Maximov, T. C. (2010). Sap flow changes in relation to permafrost degradation under increasing precipitation in an eastern Siberian larch forest. *Ecology*, *7*, 177–187.
- Kanevskiy, M., Shur, Y., Jorgenson, M. T., Ping, C., Michaelson, G. J., Fortier, D., ... Tumskov, V. (2013). Ground ice in the upper permafrost of the Beaufort Sea coast of Alaska. *Cold Regions Science and Technology*, *85*, 56–70. <https://doi.org/10.1016/j.coldregions.2012.08.002>
- Kim, Y. (2015). Effect of thaw depth on fluxes of CO₂ and CH₄ in manipulated Arctic coastal tundra of Barrow, Alaska. *Science of the Total Environment*, *505*, 385–389. <https://doi.org/10.1016/j.scitotenv.2014.09.046>
- Kumar, J., Collier, N., Bisht, G., Mills, R. T., Thornton, P. E., Iversen, C. M., & Romanovsky, V. (2016). Modeling the spatiotemporal variability in subsurface thermal regimes across a low-relief polygonal tundra landscape. *The Cryosphere*, *10*(5), 2241–2274. <https://doi.org/10.5194/tc-10-2241-2016>
- Liljedahl, A. K., Hinzman, L. D., & Schulla, J. (2012). Ice-wedge polygon type controls low-gradient watershed-scale hydrology. In K. M. Hinkel (Ed.), *Tenth international conference on permafrost, International Contributions* (Vol. 1, pp. 231–236). Salekhard, Russia: The Northern Publisher.
- Luo, D., Wu, Q., Jin, H., Marchenko, S. S., Lu, L., & Gao, S. (2016). Recent changes in the active layer thickness across the northern hemisphere. *Environment and Earth Science*, *75*(7), 555. <https://doi.org/10.1007/s12665-015-5229-2>
- Mezbahuddin, M., Grant, R. F., & Hirano, T. (2014). Modelling effects of seasonal variation in water table depth on net ecosystem CO₂ exchange of a tropical peatland. *Biogeosciences*, *11*(3), 577–599. <https://doi.org/10.5194/bg-11-577-2014>
- Moon, J.-W., & Graham, D. E. (2016). Soil water characteristics of cores from low- and high-centered polygons, Barrow, Alaska, 2012. Next Generation Ecosystem Experiments Arctic Data Collection, Carbon Dioxide Information Analysis Center, Oak Ridge National Laboratory, Oak Ridge, TN. <https://doi.org/10.5440/1299259>
- Olivas, P. C., Oberbauer, S. F., Tweedie, C., Oechel, W. C., Lin, D., & Kuchy, A. (2011). Effects of fine-scale topography on CO₂ flux components of Alaskan coastal plain tundra: Response to contrasting growing seasons. *Arctic, Antarctic, and Alpine Research*, *43*(2), 256–266. <https://doi.org/10.1657/1938-4246-43.2.256>
- Painter, S. L., Coon, E. T., Atchley, A. L., Berndt, M., Garimella, R., Moulton, J. D., ... Wilson, C. J. (2016). Integrated surface/subsurface permafrost thermal hydrology: Model formulation and proof-of-concept simulations. *Water Resources Research*, *52*, 6062–6077. <https://doi.org/10.1002/2015WR018427>
- Slater, J. G., Jaupart, C., & Galson, D. (1980). The heat flow through oceanic and continental crust and the heat loss of the Earth. *Reviews of Geophysics and Space Physics*, *18*(1), 269–311. <https://doi.org/10.1029/RG018i001p0269>
- Sommerkorn, M. (2008). Micro-topographic patterns unravel controls of soil water and temperature on soil respiration in three Siberian tundra systems. *Soil Biology and Biochemistry*, *40*(7), 1792–1802. <https://doi.org/10.1016/j.soilbio.2008.03.002>
- Torn, M., Raz-Yaseef, N., & Billesbach, D. (2016). Eddy-covariance and auxiliary measurements, NGE-Barrow, 2012–2013. Retrieved from <http://ngee-arctic.ornl.gov/>, accessed 5.6.2016.
- Vaughn, L. J. S., Conrad, M. E., Bill, M., & Torn, M. S. (2015). Isotopic insights into methane production, oxidation, and emissions in Arctic polygon tundra. *Global Change Biology*, *22*(10), 3487–3502. <https://doi.org/10.1111/gcb.13281>
- Wainwright, H. M., Dafflon, B., Smith, L. J., Hahn, M. S., Curtis, J. B., Wu, Y., ... Hubbard, S. S. (2015). Identifying multiscale zonation and assessing the relative importance of polygon geomorphology on carbon fluxes in an Arctic tundra ecosystem. *Journal of Geophysical Research: Biogeosciences*, *120*, 788–808. <https://doi.org/10.1002/2014JG002799>
- Wainwright, H. M., Liljedahl, A. K., Dafflon, B., Craig, U., Peterson, J. E., Gusmeroli, A., & Hubbard, S. S. (2017). Mapping snow depth within a tundra ecosystem using multiscale observations and Bayesian methods. *The Cryosphere*, *11*(2), 857–875. <https://doi.org/10.5194/tc-11-857-2017>
- Woo, M. K., & Guan, X. J. (2006). Hydrological connectivity and seasonal storage change of tundra ponds in a polar oasis environment, Canadian High Arctic. *Permafrost and Periglacial Processes*, *17*(4), 309–323. <https://doi.org/10.1002/ppp.565>
- Wood, S., Curtis, J. B., Norby, R., Liebig, J., Iversen, C., Sloan, V., ... Hahn, M. (2015). Soil temperature, soil moisture and thaw depth, Barrow, Alaska, Ver. 1. Retrieved from <http://ngee-arctic.ornl.gov/>, accessed 19.11.2015.
- Xu, X., & Yuan, F. (2016). Meteorological forcing at Barrow AK 1981–2013. Retrieved from <http://ngee-arctic.ornl.gov/>, accessed 22 June 2016.
- Zona, D., Lipson, D. A., Zulueta, R. C., Oberbauer, S. F., & Oechel, W. C. (2011). Microtopographic controls on ecosystem functioning in the Arctic Coastal Plain. *Journal of Geophysical Research*, *116*, G00108. <https://doi.org/10.1029/2009JG001>
- Zona, D., Oechel, W. C., Kochendorfer, J., Paw U, K. T., Salyuk, A. N., Olivas, P. C., ... Lipson, D. A. (2009). Methane fluxes during the initiation of a large-scale water table manipulation experiment in the Alaskan Arctic tundra. *Global Biogeochemical Cycles*, *23*, GB2013. <https://doi.org/10.1029/2009GB003487>